

Stellar cooling, inelastic dark matter, and XENON

Wai-Yee Keung¹, Danny Marfatia², and Po-Yan Tseng³

¹ *Department of Physics, University of Illinois at Chicago, Illinois 60607 USA*

² *Department of Physics & Astronomy, University of Hawaii at Manoa, Honolulu, HI 96822, USA*

³ *Department of Physics and IPAP, Yonsei University, Seoul 03722, Republic of Korea*

ABSTRACT: We consider a novel scenario of dark photon-mediated inelastic dark matter to explain the white dwarf cooling excess suggested by its luminosity function, and the excess in electron recoil events at XENON1T. In the Sun, the dark photon A' is produced mainly via thermal processes, and the heavier dark matter χ_2 is produced by the scattering of halo dark matter χ_1 with electrons. The XENON1T signal arises primarily by solar A' scattering, and A' emission by white dwarfs accommodates the extra cooling while maintaining consistency with other stellar cooling observations. A tritium component in the XENON1T detector is also required. We show for parameters that explain the XENON1T data, but not the white dwarf cooling anomaly, that a second signal peak may be buried in the XENON1T data and revealable at XENONnT. However, the parameters that give the double peak in the spectrum are incompatible with constraints from horizontal branch stars.

Contents

1	Introduction	1
2	Dark photon-mediated inelastic dark matter	2
2.1	$\Delta m_\chi, 40 \text{ keV} < m_{A'}$	2
2.2	$1 \text{ keV} < m_{A'} < \Delta m_\chi, 10 \text{ keV}$	6
2.3	$\Delta m_\chi < m_{A'} < 40 \text{ keV}$	9
2.3.1	Double-peak signal at XENONnT	9
3	Summary	11

1 Introduction

Astrophysical observations of several stellar systems including white dwarfs (WDs) [1–6] and horizontal branch (HB) stars [7] show evidence of excess cooling in comparison to standard theoretical predictions. The number density of WDs as a function of brightness, called the white dwarf luminosity function (WDLF), indicates a cooling anomaly at the 4σ level [8]. Pulsating WDs with a DA spectral type also show a cooling anomaly [5, 6]. The measured value of the R -parameter, which is the ratio of the number of stars in the HB to that in the upper portion of the RGB (Red Giant Branch) in globular clusters, is smaller than predicted, hinting that HB stars cool more efficiently than expected [7]. However, HB stars (aside from the aforementioned hints), RGB stars (because of their higher core temperatures) and the Sun (whose observed luminosity is consistent with the standard solar model) restrict excess cooling.

Recently, the XENON1T experiment with its 1024 kg fiducial volume and 0.65 ton-year exposure of xenon [9] reported a 3σ excess in the electron recoil spectrum between 2-3 keV. Various explanations have been put forward [10].

We propose a joint explanation of the WDLF cooling and XENON1T excesses in the context of inelastic dark matter (DM) [11] mediated by dark photons [12]; for similar scenarios in connection with XENON1T data see Refs. [13–17]. We consider two relic Majorana fermion DM particles χ_1 and χ_2 of MeV mass that form a pseudo-Dirac pair with a small mass gap, $\Delta m_\chi \equiv m_{\chi_2} - m_{\chi_1} \approx \text{keV}$. A dark photon A' of sub-GeV mass mediates the interaction between χ_1 and χ_2 . The DM halo is constituted primarily by χ_1 for the parameter values of our scenario [16]. These new particles connect the WDLF anomaly and XENON1T excess. Both χ_2 and A' can be produced in the thermal plasma of the Sun, and contribute to the XENON1T signal. The χ_2 in the Sun are created by the relic χ_1 through the process $\chi_1 e \rightarrow \chi_2 e$. A' production is dominated by bremsstrahlung [18, 19]. After propagation from the Sun to Earth, the down scattering $\chi_2 e \rightarrow \chi_1 e$ and absorption $A' e \rightarrow e$ processes yield the electron recoil signals in XENON1T. We find a region of parameter space

avored by both the WDLF anomaly and XENON1T excess, and that is consistent with constraints from other stellar cooling observations, provided a small contribution from the β -decay of tritium is present. It is noteworthy that scenarios invoking solar axion-like particles to explain the XENON1T excess are not consistent with constraints from stellar cooling, especially the R -parameter [20].

The paper is organized as follows. In section 2, we study our dark photon-mediated inelastic DM scenario and demonstrate that if $m_{A'} < \Delta m_\chi$, 10 keV both excesses can be explained. In section 2.3.1, we show that a distinctive double-peak signal may be present in XENON1T data and that can be confirmed by XENONnT. We summarize in section 3.

2 Dark photon-mediated inelastic dark matter

A' couples to χ_1, χ_2 and the electron via the effective interactions,

$$\mathcal{L} \supset (\epsilon e) A'_\mu (\bar{e} \gamma^\mu e) + \left(\frac{i g_\chi}{2} A'_\mu (\bar{\chi}_2 \gamma^\mu \chi_1) + \text{h.c.} \right), \quad (2.1)$$

where the $A'ee$ coupling may originate from the kinetic mixing between A' and the photon via $-\frac{\epsilon}{2} F'_{\mu\nu} F^{\mu\nu}$ [21]. Both $A'_\mu (\bar{\chi}_2 \gamma^\mu \chi_1)$ and its Hermitian conjugate contribute to the XENON1T signal due to their Majorana property. We insert the imaginary unit i so that g_χ is a real number.

2.1 $\Delta m_\chi, 40 \text{ keV} < m_{A'}$

Since $m_{A'} > \Delta m_\chi$, the 2-body decay $\chi_2 \rightarrow A' \chi_1$ is kinematically forbidden, and χ_2 is stable on the length scale of the solar system. The signal in XENON1T data is produced by the down scattering process,

$$\chi_2 + e \rightarrow \chi_1 + e. \quad (2.2)$$

We assume $\Delta m_\chi \simeq 3 \text{ keV}$ to obtain a peak in the XENON1T electron recoil spectrum at around 3 keV [9]. The central region of the Sun which has a keV temperature electron plasma excites χ_1 from the DM halo to produce a flux of χ_2 via

$$\chi_1 + e \rightarrow \chi_2 + e. \quad (2.3)$$

The rate for this process is given by [22, 23]

$$C_c = \frac{\rho_{\chi_1}}{m_{\chi_1}} \sum_{i=1,2,3} N_e^i \int du \frac{f_{\text{DM}}(u)}{u} (u^2 + (v_{\text{esc}}^i)^2) g_1(u) \int f_e(K_e, T^i) \sigma_{\chi_1 e \rightarrow \chi_2 e} dK_e, \quad (2.4)$$

where we divide the Sun into three shells with $i = 1, 2, 3$ corresponding to $0 \leq R < 0.1R_\odot$, $0.1R_\odot \leq R < 0.18R_\odot$, and $0.18R_\odot \leq R < 0.35R_\odot$, respectively, and sum over the contributions. Here, $N_e^i \simeq 9 \times 10^{55}, 2.1 \times 10^{56}, 4.7 \times 10^{56}$ are the number of electrons in each shell and $v_{\text{esc}}^i (\text{km/s}) = 1335, 1226, 1040$ are the corresponding escape velocities from

the outer surface of each shell, $\rho_{\chi_1} = 0.4 \text{ GeV/cm}^3$ is the local DM density,¹ and f_{DM} is the Maxwell-Boltzmann velocity distribution of DM with dispersion 270 km/s. The capture probability $g_1(u)$ depends on the energy loss distribution $(1/\sigma)d\sigma/d\Omega_{\text{CM}}$, which need not be uniform if the mediator is lighter than either of the scattered particles [22]. The Boltzmann distribution of electrons with kinetic energy K_e is

$$f_e(K_e, T^i) = 2\sqrt{\frac{K_e}{\pi}} \left(\frac{1}{T^i}\right)^{3/2} e^{-K_e/T^i},$$

where $T^i/\text{keV} \simeq 1.21, 1.02, 0.74$ are the average temperatures in each shell. The contribution to the capture rate for radii larger than $0.35R_\odot$ is negligible because of the falling temperature and exponentially falling electron number density. The total rate cannot exceed the geometric limit for the solar region within $0.35R_\odot$ [24],

$$C^\odot|_{\text{geom}} = \frac{5.4 \times 10^{29}}{\text{s}} \frac{\rho_{\chi_1}}{\text{GeV/cm}^3} \frac{\text{GeV}}{m_{\chi_1}}, \quad (2.5)$$

because in this limit all DM particles within the geometric area of the solar core are captured. For $C_c > C^\odot|_{\text{geom}}$, we take $C_c = C^\odot|_{\text{geom}}$.

The amplitude squared for $e(p_1) + \chi_1(p_2) \rightarrow e(p_3) + \chi_2(p_4)$ is given by

$$\begin{aligned} \frac{1}{4} \sum |M|^2 = & \frac{(\epsilon e g_\chi)^2}{(t - m_{A'}^2)^2} \{ 2t^2 + 4st + 4s^2 - 2(t + 2s)(m_{\chi_1}^2 + m_{\chi_2}^2) \\ & + 4tm_{\chi_1}m_{\chi_2} + 4m_{\chi_1}^2m_{\chi_2}^2 + 4m_e^2(m_e^2 - 2s + 2m_{\chi_1}m_{\chi_2}) \}. \end{aligned} \quad (2.6)$$

In the χ_1 rest frame, we define K_e and K_{χ_2} to be the kinetic energy of the incoming electron and outgoing χ_2 , respectively. Then, the Mandelstam variables can be written as

$$\begin{aligned} s &= m_{\chi_1}^2 + m_e^2 + 2m_{\chi_1}(m_e + K_e), \\ t &= m_{\chi_1}^2 + m_{\chi_2}^2 - 2m_{\chi_1}(m_{\chi_2} + K_{\chi_2}). \end{aligned} \quad (2.7)$$

The range, $K_{\chi_2}^{\min} \leq K_{\chi_2} \leq K_{\chi_2}^{\max}$, is determined from [25]

$$t = (p_1 - p_3)^2 = 2m_e^2 - 2 \left(\sqrt{m_e^2 + p_{\text{in}}^2} \sqrt{m_e^2 + p_{\text{out}}^2} - p_{\text{in}} p_{\text{out}} \cos \theta_* \right), \quad (2.8)$$

where the scattering angle in the center-of-mass frame takes values $0 \leq \theta_* \leq \pi$. Here, p_{in} (p_{out}) is the momentum of the initial (final) state in the center-of-mass frame. The cross section is given by

$$\sigma_{\chi_1 e \rightarrow \chi_2 e} = \int_{K_{\chi_2}^{\min}}^{K_{\chi_2}^{\max}} dK_{\chi_2} \frac{2m_{\chi_2}}{16\pi\lambda(s, m_e^2, m_{\chi_1}^2)} \frac{1}{4} \sum |M|^2. \quad (2.9)$$

Note that in the static limit, justified by the non-relativistic velocity of the relic dark matter, the matrix element squared can be simplified to

$$\frac{1}{4} \sum |M|^2 = (\epsilon e g_\chi)^2 \frac{(2m_e + \Delta m_\chi)^2 (2m_{\chi_1} + \Delta m_\chi)^2}{(2m_e \Delta m_\chi + m_{A'}^2)^2}. \quad (2.10)$$

¹Absent a concrete model, we do not attempt to estimate the DM relic abundance from thermal freeze-out, and allow for non-thermal production to be determinative.

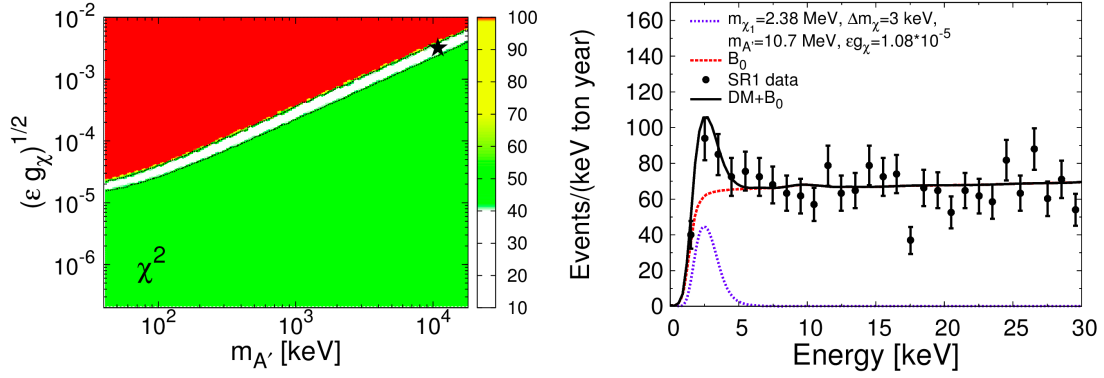


Figure 1. $m_{A'} > \Delta m_{\chi}$. The left panel shows the χ^2 distribution from a fit to XENON1T data. The 2σ contour corresponds to $\Delta\chi^2 \equiv \chi^2 - \chi_{\text{BP1}}^2 = 6.17$, where $\chi_{\text{BP1}}^2 = 35.76$ for the best-fit point **BP1** in Eq. (2.13) which is marked by a star. Its electron recoil spectra is shown in the right panel.

The χ_2 flux at the Earth, assuming that it is produced isotropically in the Sun, is obtained from

$$\frac{d\Phi_{\chi_2}}{dK_{\chi_2}} = \frac{1}{4\pi D_{\text{SE}}^2} \frac{dC_c}{dK_{\chi_2}}, \quad (2.11)$$

where the distance between the Sun and Earth, $D_{\text{SE}} \equiv 1$ AU. Subsequently, the χ_2 interacts with an electron in the XENON1T detector. The event rate for the down scattering $\chi_2 e \rightarrow \chi_1 e$ is

$$\frac{dR}{dK_r} = N_T^e \int \frac{d\Phi_{\chi_2}}{dK_{\chi_2}} \frac{d\sigma_{\chi_2 e \rightarrow \chi_1 e}}{dK_r}, \quad (2.12)$$

where K_r is the electron recoil energy and N_T^e is the total effective number of target electrons in the XENON1T detector. Because only the outer shell electrons, from the $4s$ to $5p$ orbitals of Xe have a binding energy less than keV, we take 26 electrons for each Xe atom [26]. We fold in the detector efficiency [9] and energy resolution [13] functions to compute the event spectrum.

We fit the 29 bins of the XENON1T spectrum between 1 keV and 30 keV obtained during Science Run 1 (SR1) by scanning over m_{χ_1} , $m_{A'}$ and ϵg_{χ} , and find the best fit point,

$$\mathbf{BP1} : (m_{\chi_1}, \Delta m_{\chi}, m_{A'}, \epsilon g_{\chi}) = (2.38 \text{ MeV}, 3 \text{ keV}, 10.7 \text{ MeV}, 1.08 \times 10^{-5}), \quad (2.13)$$

with $\chi_{\text{BP1}}^2 = 35.76$. The background-only hypothesis B_0 [9] has $\chi_{B_0}^2 = 46.69$. The χ^2 distribution in the $(m_{A'}, \sqrt{\epsilon g_{\chi}})$ plane is shown in the left panel of Fig. 1, which displays a strong correlation between $m_{A'}$ and ϵg_{χ} . The spectrum of **BP1** is shown in the right panel.

In principle, a light A' can be thermally produced in the hot electron plasma of the Sun via the coupling ϵe . Such a solar A' flux can produce the recoil electrons responsible for the XENON1T excess. However, for $m_{A'} > 40$ keV, the A' contribution is severely Boltzmann suppressed.

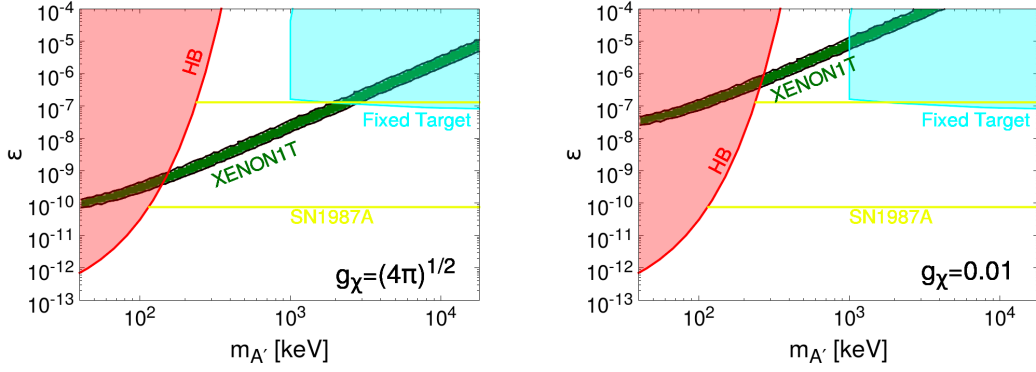


Figure 2. $m_{A'} > \Delta m_\chi$. The 2σ XENON1T allowed regions for $g_\chi = \sqrt{4\pi}$ and $g_\chi = 0.01$ with $m_{\chi_1} = 5$ MeV. The constraints from HB stars [18, 19], fixed-target experiments [27] and an approximate constraint from SN 1987A [28] are also shown.

In Fig. 2, we overlay the XENON1T preferred regions for $g_\chi = \sqrt{4\pi}$ and 0.01 with constraints from HB stars [18, 19], fixed-target experiments [27] and supernova 1987A [28]. The unshaded region labelled “SN1987A” is an approximate representation of the region constrained by SN 1987A. A detailed analysis is necessary to define the region precisely. For $g_\chi = \sqrt{4\pi}$ the XENON1T preferred region is excluded, and for $g_\chi = 0.01$, the allowed window is $0.3 \text{ MeV} \lesssim m_{A'} \lesssim 1 \text{ MeV}$. However, the number of effective number of relativistic neutrinos at recombination, N_{eff} , is sensitive to $m_{A'} \lesssim 1 \text{ MeV}$ and $\epsilon \gg 10^{-8}$ [29]. The processes, $A' + \gamma \leftrightarrow e^- + e^+$ and $A' + e^\pm \leftrightarrow \gamma + e^\pm$, heat up only the electron-photon plasma and reduce N_{eff} to $\simeq 1.7$, which is excluded by cosmic microwave background data [29].

The shape of the WDLF can be expressed as a simple power law if neutrino cooling is negligible [8]:

$$L_\gamma = 8.5 \times 10^{-4} L_\odot \left(\frac{T_{\text{WD}}}{10^7 \text{ K}} \right)^{3.5}, \quad (2.14)$$

where the solar luminosity is $L_\odot = 2.39 \times 10^{36} \text{ GeV/s}$. The exotic cooling rate of the WD can be similarly parametrized as

$$L_X = C_X L_\odot \left(\frac{T_{\text{WD}}}{10^7 \text{ K}} \right)^n. \quad (2.15)$$

A fit to the data of Ref. [4] yields the best-fit values, $C_X = 1.31 \times 10^{-4}$ and $n = 3.49$ [8]. Taking the WD core temperature to be $10^7 \text{ K} = 0.862 \text{ keV}$,

$$L_X \simeq 3.13 \times 10^{32} \text{ GeV/s}. \quad (2.16)$$

The relic DM χ can cool the WD through the process $\chi_1 e \rightarrow \chi_2 e$. However, even at the geometric limit its rate is $2.2 \times 10^{26} \text{ GeV/s}$ for $m_{\chi_1} \simeq \mathcal{O}(\text{MeV})$ and $\Delta m_\chi \simeq \mathcal{O}(\text{keV})$, which is six orders of magnitude below the required anomalous rate of Eq. (2.16).

2.2 $1 \text{ keV} < m_{A'} < \Delta m_\chi, 10 \text{ keV}$

We now consider $m_{A'} < \Delta m_\chi$ so that once χ_2 is produced inside the Sun via $\chi_1 e \rightarrow \chi_2 e$, it decays promptly: $\chi_2 \rightarrow A' \chi_1$. Then, none of the χ_2 propagate to Earth to generate a XENON1T signal. The amplitude squared and decay width are given by

$$\begin{aligned} \frac{1}{2} \sum |M_{\chi_2 \rightarrow A' \chi_1}|^2 &= g_\chi^2 \left\{ m_{\chi_2}^2 - 6m_{\chi_1} m_{\chi_2} + m_{\chi_1}^2 - 2m_{A'}^2 + \frac{1}{m_{A'}^2} (m_{\chi_2}^2 - m_{\chi_1}^2)^2 \right\} \\ \Gamma_{\chi_2 \rightarrow A' \chi_1} &= \frac{1}{16\pi m_{\chi_2}} \frac{1}{2} \sum |M_{\chi_2 \rightarrow A' \chi_1}|^2 \lambda^{1/2} \left(1, \frac{m_{\chi_1}^2}{m_{\chi_2}^2}, \frac{m_{A'}^2}{m_{\chi_2}^2} \right). \end{aligned} \quad (2.17)$$

The $(m_{\chi_2}^2 - m_{\chi_1}^2)^2/m_{A'}^2$ term in the amplitude squared arises from the longitudinal component of A' , and dominates when $m_{A'} \ll \Delta m_\chi$.

The A' easily escapes the Sun, propagates to Earth, and contributes to the electron recoil signal at XENON1T through absorption by the bound electrons of Xe, $A' e \rightarrow e$, analogous to the photoelectric effect. The A' absorption cross section per Xe atom is

$$\sigma_{A'} \begin{cases} \simeq \left(\frac{m_{A'}}{\omega}\right)^2 \epsilon^2 \sigma_\gamma \left(\frac{c}{v_{A'}}\right) & \text{for longitudinal } A', \\ = \epsilon^2 \sigma_\gamma \left(\frac{c}{v_{A'}}\right) & \text{for transverse } A' \text{ [30]}, \end{cases} \quad (2.18)$$

where $v_{A'}$ is the A' velocity, and σ_γ is the photoelectric cross section per Xe atom which is a function of the A' energy ω [31, 32]. Note the $(m_{A'}/\omega)^2$ suppression for longitudinal modes. Since χ_2 with kinetic energy of $\mathcal{O}(\text{keV})$ is non-relativistic, A' from χ_2 decay has energy $\omega \simeq \Delta m_\chi$. The A' flux is identical to the χ_2 flux and can be obtained from Eq. (2.11):

$$\Phi_{A'}^{\chi_2}|_{\omega=\Delta m_\chi} = \int dK_{\chi_2} \frac{d\Phi_{\chi_2}}{dK_{\chi_2}}.$$

The A' contribution from χ_2 decay to the XENON1T event rate can be estimated as follows. Assume the up scattering $\chi_1 e \rightarrow \chi_2 e$ in the Sun reaches the geometric limit. Then χ_2 decay produces the maximum flux, $\Phi_{A'}^{\chi_2} \simeq 7.44 \times 10^4 \text{ cm}^{-2} \text{ s}^{-1}$ for $m_{\chi_1} \simeq \mathcal{O}(\text{MeV})$. This yields an electron recoil event rate $\simeq \epsilon^2 (2 \times 10^{21}) \text{ ton}^{-1} \text{ yr}^{-1}$, which requires $\epsilon \simeq \mathcal{O}(10^{-10})$ to explain the XENON1T excess. The $(m_{A'}, \epsilon) \simeq (\mathcal{O}(1 \text{ keV}), \mathcal{O}(10^{-10}))$ region of parameter space is ruled out by cooling constraints from the Sun and HB stars.

However, keV mass A' are also produced by the thermal plasma of the Sun. In fact, this contribution dominates the solar A' flux. We define the A' number production rate per unit volume per unit energy as $\frac{d^2 \Gamma_{A'}^\odot}{dV d\omega}$ which depends on the plasma frequency $\omega_p = (n_e e^2/m_e)^{1/2}$ with n_e the number density of electrons. We will only be interested in A' masses above the plasma frequency $\omega_p \simeq 0.3 \text{ keV}$ in the core of the Sun with $R_{\text{core}} = 0.18 R_\odot$; in the center of HB stars, $\omega_p \simeq 2 \text{ keV}$. In this case, the number emission rate of longitudinal modes per unit volume per unit energy ω is given by [18, 19]

$$\left. \frac{d^2 \Gamma_{A'}^\odot}{dV d\omega} \right|_L = \sum_{i=H, He} \frac{8Z_i^2 \alpha^3 n_e n_{Z_i}}{3m_e^2} \frac{\epsilon^2 m_{A'}^2}{\omega^4} \sqrt{\omega^2 - m_{A'}^2} \sqrt{\frac{8m_e}{\pi T}} f(\sqrt{\omega/T}), \quad (2.19)$$

where n_{Z_i} is the number density of ions of charge $-Z_i e$ [33], and

$$f(a) \equiv \int_a^\infty dx x e^{-x^2} \log \left| \frac{x + \sqrt{x^2 - a^2}}{x - \sqrt{x^2 - a^2}} \right|. \quad (2.20)$$

The corresponding expression for the transverse modes is [34]

$$\begin{aligned} \left. \frac{d^2 \Gamma_{A'}^\odot}{dV d\omega} \right|_T &= \frac{1}{\pi^2} \frac{\omega \sqrt{\omega^2 - m_{A'}^2}}{e^{\frac{\omega}{T_\odot}} - 1} \frac{\epsilon^2 m_{A'}^4}{(\omega_p^2 - m_{A'}^2)^2 + (\omega \Gamma_T)^2} \Gamma_T, \\ \Gamma_T &= \frac{16\pi^2 \alpha^3}{3m_e^2 \omega^3} \sqrt{\frac{2\pi m_e}{3T_\odot}} n_e \sum_{i=H, He} Z_i^2 n_{Z_i} \bar{g}_i (1 - e^{-\frac{\omega}{T_\odot}}) + \frac{8\pi \alpha^2}{3m_e^2} n_e, \end{aligned} \quad (2.21)$$

where \bar{g}_i is a Boltzmann averaged Gaunt factor [35]. For $T_\odot = 1.15$ keV and $R_{\text{core}}/R_\odot = 0.18$, we find that setting $\bar{g}_H = \bar{g}_{He} = 1$ reproduces the result of Ref. [19] in the $m_{A'}$ range of interest.

The A' flux at Earth produced in the thermal plasma of the Sun is given by

$$\frac{d\Phi_{A'}^\odot}{d\omega} = \frac{1}{4\pi D_{\text{SE}}^2} \int dV \frac{d^2 \Gamma_{A'}^\odot}{dV d\omega}. \quad (2.22)$$

The A' contribution to the XENON1T spectrum is

$$\frac{dR}{d\omega} \simeq N_T \sigma_{A'} \frac{d\Phi_{A'}^\odot}{d\omega}, \quad (2.23)$$

where $N_T \simeq 4.52 \times 10^{27}$ is the number of Xe atoms per ton.

It is interesting that the best fit value of n in Eq. (2.15) is the same as in Eq. (2.14) for photon emission. This implies that the emission of a light particle like A' could provide the additional contribution to WD cooling. In the core of a WD, $\omega_p \simeq 30$ keV. For $m_{A'} \ll \omega_p$, the resonant emission of longitudinal A' is enhanced by $(\omega_p/m_{A'})^2$, can occur at any temperature, and is given by [18, 19]:

$$\frac{d^2 \Gamma_{A'}^{\text{WD}}}{dV d\omega} = \frac{1}{4\pi} \frac{\epsilon^2 m_{A'}^2 \omega^2}{e^{\omega/T} - 1} \delta(\omega - \omega_p). \quad (2.24)$$

To explain the excess WD cooling by A' emission, we require

$$\begin{aligned} L_X &= \int dV \int d\omega \omega \frac{d^2 \Gamma_{A'}^{\text{WD}}}{dV d\omega} = \left(\frac{4}{3} \pi R_{\text{WD}}^3 \right) \frac{1}{4\pi} \frac{\epsilon^2 m_{A'}^2 \omega_p^3}{e^{\omega_p/T_{\text{WD}}} - 1}, \\ \text{i.e., } \quad \epsilon m_{A'} &\simeq 10^{-14} \text{ keV}. \end{aligned} \quad (2.25)$$

For $m_{A'} \ll \omega_p$, the region favored by the WDLF is a band with slope -1 in the $\log \epsilon - \log m_{A'}$ plane; see Fig. 3. This is confirmed by numerical simulations up to $m_{A'} \simeq 1.6$ keV [8]. We have extended this band to 4 keV, above which the condition, $m_{A'} \ll \omega_p$, breaks down. For $2.5 \text{ keV} \lesssim m_{A'} \lesssim 4 \text{ keV}$, the WDLF favored region is consistent with all constraints. Note that Eqs. (2.23) and (2.25) are independent of g_χ .

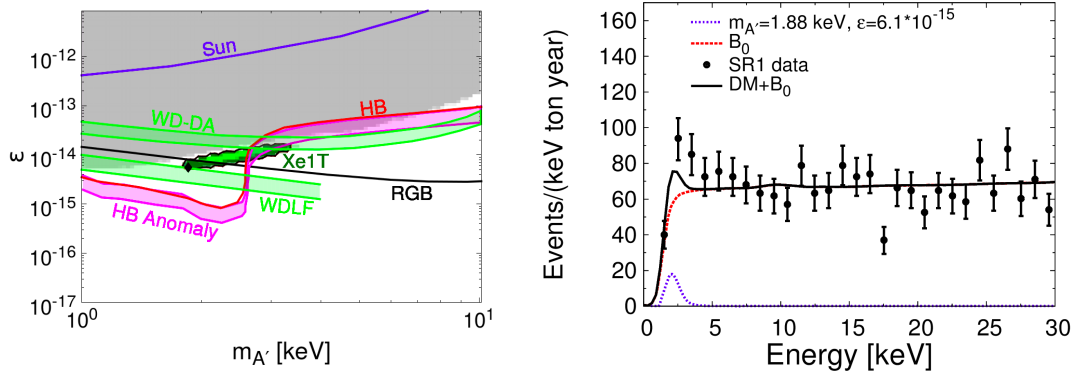


Figure 3. $m_{A'} < \Delta m_\chi$. In the left-panel, we show the parameter regions favored by the cooling excesses suggested by the WDLF (at 2σ), WDs of spectral type DA (WD-DA), and by the HB anomaly. The 1σ and 2σ allowed regions that explain the XENON1T are labelled “Xe1T”. Regions above the curves labelled, “Sun”, “HB” (red) and “RGB” are excluded at 2σ by the respective stellar constraints. The gray shaded region labelled “ $\Delta\chi^2_{\text{Xe1T}} \geq 100$ ” is strongly disfavored. The “Xe1T” and “WDLF” regions overlap in the vicinity of $(m_{A'}, \epsilon) = (1.88 \text{ keV}, 6.1 \times 10^{-15})$, marked by a diamond, and its electron recoil spectrum at XENON1T is shown in the right panel.

In Fig. 3, we show the 1σ and 2σ regions favored by XENON1T data and the 2σ region favored by the WDLF. The 2σ regions barely overlap in the vicinity of

$$\mathbf{BP2}: (m_{A'}, \epsilon) = (1.88 \text{ keV}, 6.1 \times 10^{-15}),$$

which has $\chi^2 = 42.12$ in a fit to the XENON1T data. Its electron recoil spectrum is shown in the right panel. The best-fit point $(m_{A'}, \epsilon) = (2.69 \text{ keV}, 1.26 \times 10^{-14})$ with $\chi^2_{\text{best-fit}} = 36.07$ does not explain the WDLF data and is excluded by the RGB constraint. The gray region marked “ $\Delta\chi^2_{\text{Xe1T}} \geq 100$ ” is strongly disfavored because $\chi^2 \geq 100$ for XENON1T data.

We therefore consider the possibility that a tritium component contributes to the XENON1T excess in addition to solar A' . Then, smaller values of ϵ are needed which could reconcile the WDLF excess. The result of allowing a free-floating normalization of the β -decay contribution from tritium decay is shown in Fig. 4. $F_T = 1$ sets the normalization of the tritium spectrum in Ref. [9] and yields $\chi^2_T = 41.8$, which is close to $\chi^2_{\mathbf{BP2}} = 42.12$. Including the tritium contribution with $F_T = 0.63$ improves the fit of $\mathbf{BP2}$ to $\chi^2_{\mathbf{BP2}} = 39.36$. The expanded allowed region is even compatible with the HB anomaly.

In the scenario of Ref. [13], the hidden photon is the relic DM candidate and its production in the Sun is neglected. Our preferred value of ϵ is larger than in Ref. [13] because the A' fluxes differ. For the DM A' , the A' flux is determined by the local DM number density $n_{\text{DM}} \simeq 0.3 \text{ GeV/cm}^3$ and the dispersion velocity $v_{\text{DM}} \simeq 10^{-3}c$, which gives $\Phi_{A'}^{\text{DM}}(c/v_{\text{DM}}) \simeq 3 \times 10^{15} \text{ cm}^{-2}\text{s}^{-1}$. The event rate $R_{A'}^{\text{DM}} \simeq \epsilon_{\text{DM}}^2 (\Phi_{A'}^{\text{DM}}/v_{\text{DM}}) N_T \sigma_\gamma c$ yields $(m_{A'}, \epsilon_{\text{DM}}) = (2.8 \text{ keV}, 8.6 \times 10^{-16})$ as the best fit point [13]. To compare with our model, we fix $m_{A'} = 2.8 \text{ keV}$, multiply the solar A' differential flux at the Earth by $c/v_{A'}$ and

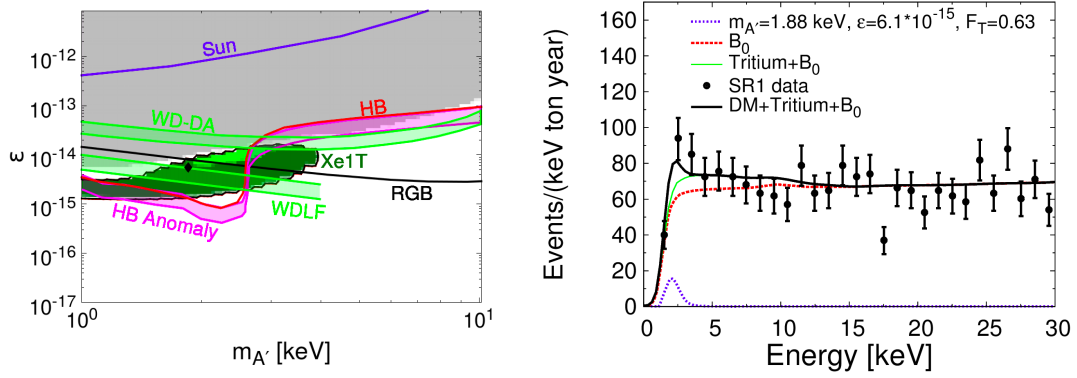


Figure 4. Same as Fig. 3, but including a tritium contribution whose normalization factor F_T is a free parameter. The right panel shows the spectrum of $(m_{A'}, \epsilon, F_T) = (1.88 \text{ keV}, 6.1 \times 10^{-15}, 0.63)$, a point that explains the WDLF and XENON1T excesses.

integrate over energy. Both scenarios should give the same event rate at XENON1T:

$$\epsilon_{\text{DM}}^2 \left(\frac{\Phi_{A'}^{\text{DM}} c}{v_{\text{DM}}} \right) = \epsilon^2 \int d\omega \frac{d\Phi_{A'}^\odot}{d\omega} \left(\frac{c}{v_{A'}} \right) \simeq \left(\frac{\epsilon}{10^{-7}} \right)^4 \times 1.67 \times 10^{13} \text{ cm}^{-2} \text{ s}^{-1}. \quad (2.26)$$

Note that the event rate $\sim \epsilon^4$ in our model because the event rate picks up two powers of ϵ each at A' production in the Sun and its interaction in the detector. An order of magnitude larger value, $\epsilon = 1.15 \times 10^{-14}$, is preferred in our scenario.

2.3 $\Delta m_\chi < m_{A'} < 40 \text{ keV}$

In the previous two subsections either χ_2 or A' produced the XENON1T signal, but not both. Here, we study a hybrid case in which both χ_2 and A' produce signals in XENON. This can occur if $\Delta m_\chi < m_{A'}$ so that χ_2 decay is forbidden, and $m_{A'}$ is light enough that it can be produced in the Sun. Because we set $\Delta m_\chi = 3 \text{ keV}$, these conditions are satisfied for $3 \text{ keV} < m_{A'} < 40 \text{ keV}$. The parameter region from an analysis of XENON1T data up to 50 keV is shown in Fig. 5. A tritium contribution is not included. A fit of the background to the 38 bins gives $\chi_{B_0}^2 = 56.06$.

2.3.1 Double-peak signal at XENONnT

The point $(m_{A'}, \epsilon, g_\chi) \simeq (39 \text{ keV}, 6.93 \times 10^{-11}, \sqrt{4\pi})$ is interesting because the two contributions from χ_2 and A' to XENON1T data are comparable. This point has $\chi^2 = 46.22$, i.e., $\Delta\chi^2 = 9.84$, which for 3 parameters gives a p -value of 0.020, so it is allowed at 98% CL. A distinctive double peak in the electron recoil spectrum is predicted, as illustrated in the left panel of Fig. 6. The peak at 3 keV is from the narrow mass gap of χ , and the peak around 39 keV is due to the solar A' of the same mass value. The signal at 39 keV is hidden in the huge background induced by the neutron-activated isotope ^{131m}Xe [9]. Note that this parameter region does not explain the WDLF anomaly and is excluded by HB cooling constraints.

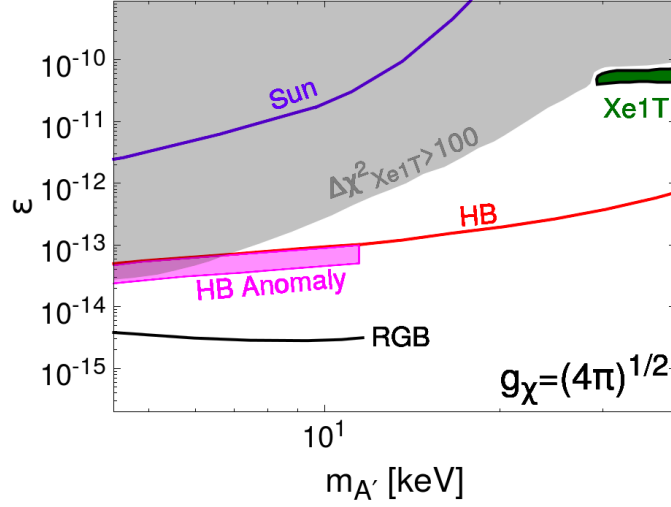


Figure 5. $\Delta m_{\chi} = 3 \text{ keV} < m_{A'} < 40 \text{ keV}$. Similar to Fig. 3, but in this hybrid case, both χ_2 and A' produce signals in XENON. In this analysis we include XENON1T data up to 50 keV and set $m_{\chi_1} = 5 \text{ MeV}$.

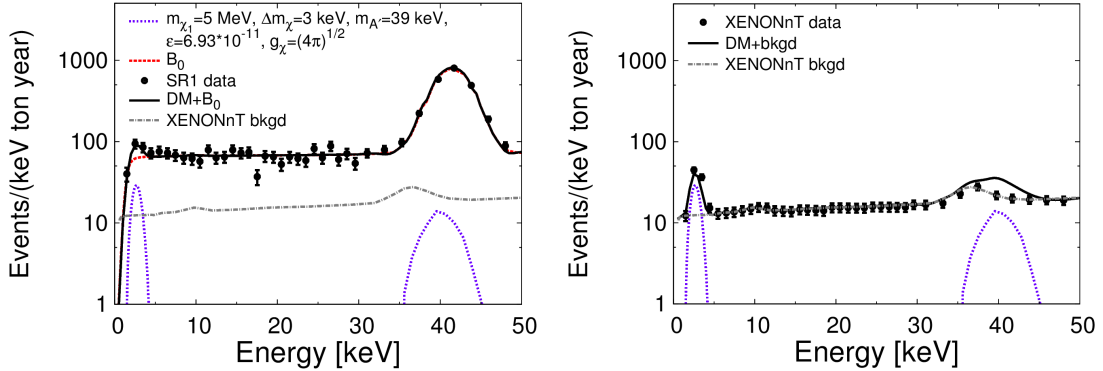


Figure 6. The double-peak spectra for the hybrid case. The left panel shows the XENON1T spectrum, and the right panel shows that both peaks will be evident in 4 ton-year of XENONnT data.

To evaluate the sensitivity of XENONnT data [36], we assume the same number of excess events per keV-ton-year as XENON1T with uncertainties reduced by a factor of 2.5 for a 4 ton-year exposure; see the right panel of Fig. 6. We also assume that xenon purification will remove tritium to an undetectable level. For the parameter point in the left panel, the signal gives $\chi^2 = 48.66$ and the background hypothesis has $\chi^2_{\text{bkgd}} = 159.59$, so the signal will be easily detected.

Next, we suppose that XENONnT does not see an excess, and the background expectation [36] in the recoil energy range, 1 keV to 13 keV, is consistent with data. Then

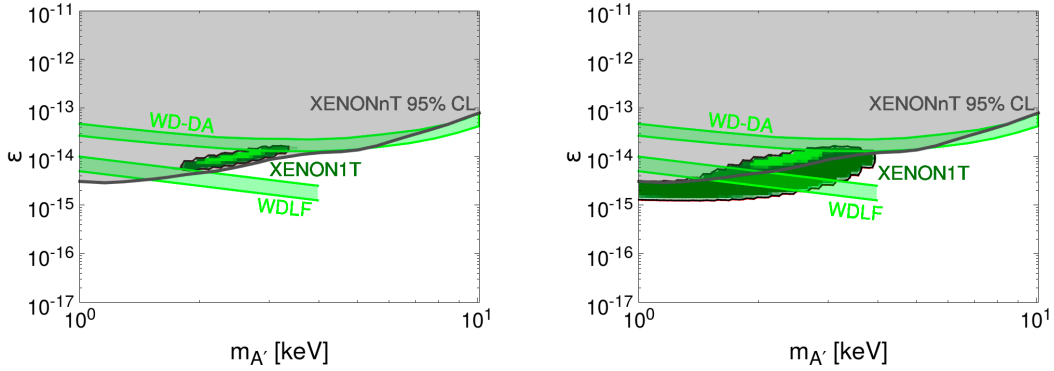


Figure 7. The expected 95% exclusion limit from XENONnT data between 1 keV and 13 keV assuming no excess is seen in 4 ton-year of XENONnT data. The XENON1T regions in the left (right) panel are from Fig. 3 (Fig. 4) without (with) a tritium component to the excess.

XENONnT data will be able to exclude the XENON1T allowed region of Fig. 3, which did not assume a tritium contribution; see the left panel of Fig. 7. From the right panel we see that XENONnT will not be able to exclude the scenario that allows for a tritium component to the XENON1T excess.

3 Summary

We proposed dark-photon mediated inelastic DM as an explanation of the WDLF cooling anomaly as well as the XENON1T electron recoil excess. The entire DM halo is composed of the lighter dark particle χ_1 , and thermal electrons inside the Sun provide a power source to excite χ_1 into χ_2 through the process, $\chi_1 e \rightarrow \chi_2 e$. For $m_{A'} \gtrsim \Delta m_\chi, 40$ keV, the stable χ_2 propagates to Earth and contributes to electron recoil events at XENON1T via the down scattering process, $\chi_2 e \rightarrow \chi_1 e$. The recoil spectrum features a peak around the mass difference between χ_1 and χ_2 , $\Delta m_\chi = 3$ keV.

For $m_{A'} < \Delta m_\chi, 10$ keV, the χ_2 produced in the Sun decays promptly to $A' \chi_1$ so that A' contributes, though subdominantly, to the XENON1T signal. The dominant A' production in the Sun arises from the thermal plasma which can explain the XENON1T excess with $(m_{A'}, \epsilon) = (1.88 \text{ keV}, 6.1 \times 10^{-15})$ provided a tritium component also contributes to the XENON1T spectrum.

For $\Delta m_\chi < m_{A'} < 40$ keV, a distinctive signature of our model is a second peak in the XENON1T spectrum that is currently not detectable. However, the parameter region where this occurs does not explain the white dwarf cooling excess and is severely constrained by HB cooling.

If the same event excess is found at XENONnT, it will be definitively confirmed. On the other hand, if XENONnT data are consistent with the background, the parameter region favored by the XENON1T anomaly (without a tritium contribution) will be ruled

out at 2σ . The preferred region common to the XENON1T and WDLF anomalies can not be fully probed by XENONnT after complete removal of tritium; see Fig. 7.

Acknowledgements

D.M. is supported in part by the U.S. DOE under Grant No. de-sc0010504. P.T is supported by National Research Foundation of Korea (NRF) funded by the Ministry of Education, Science and Technology (NRF-2020R1I1A1A01066413).

References

- [1] S. O. Kepler, D. E. Winget, R. E. Nather, P. A. Bradley, A. D. Grauer, G. Fontaine, P. Bergeron, G. Vauclair, C. F. Claver, T. M. K. Marar, *et al.*, Ap. J. **378**, L45 (1991).
- [2] J. Isern, M. Hernanz and E. Garcia-Berro, *Astrophys. J. Lett.* **392**, L23 (1992)
- [3] M. M. Miller Bertolami, B. E. Melendez, L. G. Althaus and J. Isern, JCAP **10**, 069 (2014) [arXiv:1406.7712 [hep-ph]].
- [4] M. M. Miller Bertolami, *Astron. Astrophys.* **562**, A123 (2014) doi:10.1051/0004-6361/201322641 [arXiv:1407.1404 [hep-ph]].
- [5] A. H. Corsico, L. G. Althaus, M. M. M. Bertolami, A. D. Romero, E. Garcia-Berro, J. Isern and S. O. Kepler, *Mon. Not. Roy. Astron. Soc.* **424**, 2792 (2012) [arXiv:1205.6180 [astro-ph.SR]].
- [6] A. H. Corsico, L. G. Althaus, A. D. Romero, A. S. Mukadam, E. Garcia-Berro, J. Isern, S. O. Kepler and M. A. Corti, JCAP **12**, 010 (2012) [arXiv:1211.3389 [astro-ph.SR]].
- [7] A. Ayala, I. Dominguez, M. Giannotti, A. Mirizzi and O. Straniero, *Phys. Rev. Lett.* **113**, no.19, 191302 (2014) [arXiv:1406.6053 [astro-ph.SR]].
- [8] M. Giannotti, I. Irastorza, J. Redondo and A. Ringwald, JCAP **1605**, 057 (2016), [arXiv:1512.08108 [astro-ph.HE]].
- [9] E. Aprile *et al.* [XENON Collaboration], arXiv:2006.09721 [hep-ex].
- [10] For an extensive list see the citations to [9].
- [11] D. Tucker-Smith and N. Weiner, *Phys. Rev. D* **64**, 043502 (2001) [arXiv:hep-ph/0101138 [hep-ph]].
- [12] B. Batell, M. Pospelov and A. Ritz, *Phys. Rev. D* **79**, 115019 (2009) [arXiv:0903.3396 [hep-ph]].
- [13] G. Alonso-Álvarez, F. Ertas, J. Jaeckel, F. Kahlhoefer and L. J. Thormaehlen, JCAP **11**, 029 (2020) [arXiv:2006.11243 [hep-ph]].
- [14] K. Harigaya, Y. Nakai and M. Suzuki, *Phys. Lett. B* **809**, 135729 (2020) [arXiv:2006.11938 [hep-ph]].
- [15] M. Baryakhtar, A. Berlin, H. Liu and N. Weiner, [arXiv:2006.13918 [hep-ph]].
- [16] J. Bramante and N. Song, *Phys. Rev. Lett.* **125**, no. 16, 161805 (2020), [arXiv:2006.14089 [hep-ph]].
- [17] I. M. Bloch, A. Caputo, R. Essig, D. Redigolo, M. Sholapurkar and T. Volansky, [arXiv:2006.14521 [hep-ph]].

- [18] H. An, M. Pospelov and J. Pradler, Phys. Lett. B **725**, 190 (2013), [arXiv:1302.3884 [hep-ph]].
- [19] J. Redondo and G. Raffelt, JCAP **1308**, 034 (2013), [arXiv:1305.2920 [hep-ph]].
- [20] L. Di Luzio, M. Fedele, M. Giannotti, F. Mescia and E. Nardi, Phys. Rev. Lett. **125**, no.13, 131804 (2020) [arXiv:2006.12487 [hep-ph]].
- [21] B. Holdom, Phys. Lett. B **166**, 196-198 (1986)
- [22] B. Dasgupta, A. Gupta and A. Ray, arXiv:2006.10773 [hep-ph].
- [23] S. D. McDermott, H. B. Yu and K. M. Zurek, Phys. Rev. D **85**, 023519 (2012), [arXiv:1103.5472 [hep-ph]].
- [24] R. Garani, Y. Genolini and T. Hambye, JCAP **1905**, 035 (2019), [arXiv:1812.08773 [hep-ph]].
- [25] Y. Jho, J. C. Park, S. C. Park and P. Y. Tseng, Phys. Lett. B **811**, 135863 (2020) [arXiv:2006.13910 [hep-ph]].
- [26] Q. H. Cao, R. Ding and Q. F. Xiang, arXiv:2006.12767 [hep-ph].
- [27] R. Harnik, J. Kopp and P. A. N. Machado, JCAP **1207**, 026 (2012), [arXiv:1202.6073 [hep-ph]].
- [28] J. H. Chang, R. Essig and S. D. McDermott, JHEP **09**, 051 (2018) [arXiv:1803.00993 [hep-ph]].
- [29] M. Ibe, S. Kobayashi, Y. Nakayama and S. Shirai, JHEP **2004**, 009 (2020), [arXiv:1912.12152 [hep-ph]].
- [30] M. Pospelov, A. Ritz and M. B. Voloshin, Phys. Rev. D **78**, 115012 (2008), [arXiv:0807.3279 [hep-ph]].
- [31] K. Arisaka *et al.*, Astropart. Phys. **44**, 59 (2013), [arXiv:1209.3810 [astro-ph.CO]].
- [32] M. Fabbrichesi, E. Gabrielli and G. Lanfranchi, arXiv:2005.01515 [hep-ph].
- [33] J. N. Bahcall and R. K. Ulrich, Rev. Mod. Phys. **60**, 297 (1988).
- [34] J. Redondo, JCAP **0807**, 008 (2008), [arXiv:0801.1527 [hep-ph]].
- [35] P. J. Brussaard and H. C. van de Hulst, Rev. Mod. Phys. **34**, 507 (1962).
- [36] E. Aprile *et al.* [XENON], JCAP **11**, 031 (2020) [arXiv:2007.08796 [physics.ins-det]].